Measuring the intrarenal distribution of glomerular volumes from histological sections

A thesis submitted to the graduate division of the University of Hawai'i at Mānoa in partial fulfillment of the requirements for the degree of Master of Science in Molecular Biosciences and Bioengineering

May 2017

Bradley D. Hann

Thesis committee:
Kevin Bennett (chairperson), Daniel Jenkins, Gernot Presting

May 2017

Contents

List of Figures and Tables

Disclaimer

Although it is traditional to publish data after the submission of a MS Thesis, this work was published prior to submission of the MS Thesis as:

Measuring the intra-renal distribution of glomerular volumes from histologic sections

Bradley D Hann, Edwin J Baldelomar, Jennifer R. Charlton, Kevin M. Bennett

American Journal of Physiology - Renal Physiology Mar 2016, ajprenal.00382.2015; ***DOI:*** *10.1152/ajprenal.00382.2015.*

That work was designed, performed, analyzed, written, edited, and published by Bradley Hann while a student at University of Hawaii at Manoa. Notable contributions from coauthors includes:

E. Baldelomar

- Consulted in the initial design and conception of the experiment.
- Performed and analyzed the MRI experiments described in Chapter 2.
- Assisted with manual image segmentation.
- Consulted in the interpretation of results.
- Edited and approved the AJP manuscript.

J. Charlton

- Consulted in the initial design and conception of the experiment.
- Provided whole kidneys from WT and Os/$^{+}$ mice.
- Consulted in the interpretation of results.
- Edited and approved the AJP manuscript.

K. Bennett

- Consulted in the initial design and conception of the experiment.
- Consulted in the interpretation of results.
- Edited and approved the AJP manuscript.
- Edited and approved this Thesis.

This thesis draws heavily on the AJP manuscript, including blocks of text, figures, and tables. The figures and initial draft of the AJP manuscript were prepared solely by Bradley Hann while a student at UH Manoa.

Introduction

The kidney has a significant ability to adapt to acute and chronic stress. However, unremitting stimulation of the renal adaptive mechanisms eventually contributes to the progression of disease. Renal adaptive mechanisms are highlighted clinically by the kidney's ability to maintain a stable glomerular filtration rate with a wide range in the number of functioning nephrons(1). Because human nephron number is determined at birth and decreases with ageing (2,3), glomerular hypertrophy is one response the kidney employs to adapt and provide a constant filtration surface area when there are too few nephrons to maintain the homeostatic function of the kidney.

Glomerular hypertrophy is manifested in a number of diseases such as diabetes, obesity, pregnancy, autosomal dominant polycystic kidney disease, focal segmental glomerulosclerosis, and following acute kidney injury(4). Although many types of glomerular hyperfiltration lead to glomerular hypertrophy and glomerulosclerosis, the specific mechanisms depend on the pathology(5) and the damage is heterogeneously distributed throughout the kidney (6). Importantly, disease progression is often heterogeneously observed in individual kidneys, particularly at the earliest stages, and focal changes may not present in estimates of average glomerular volume. Early detection of glomerular hypertrophy in patients or preclinical models may enable targeted therapy earlier in disease progression, improving the chances of halting the progression of chronic kidney disease. Thus, an efficient technique to examine the distribution of glomerular volumes is critical.

Stereological techniques are used to estimate the number (N_{glom}) and average volume of glomeruli (AV_{glom}) and other structures. Stereology is typically performed by thinly sectioning the kidney and measuring the number and area of glomeruli visible in a fraction of those slices. A mathematical model, based on certain simplifying assumptions, is used to extrapolate the N_{glom} from the profile measurements. One model-based method, outlined by Weibel and Gomez in 1962(7), assumes that glomeruli are spheres with radii that are normally distributed in the kidney. An alternative method, the unbiased fractioner/dissector, is generally preferred over model-based methods in studies in humans (8-10). The fractionator/dissector method dispenses with the geometric assumptions of Weibel and Gomez but requires sampling pairs of tissue slices and counting profiles that appear in only one section of the pair. Another, new strategy for measuring glomerular endowment relies on injecting a cationic magnetic resonance imaging (MRI) contrast agent that binds to the anionic glomerular basement membrane (11-15). The number of functioning glomeruli can be determined by counting the resulting dark artifacts in an MR image.

In this work, we develop a stereological technique to measure the intra-renal distribution of individual glomerular volume (IV_{glom}) and the standard deviation of intra-renal glomerular volumes, σ_{glom}, in addition to AV_{glom} and N_{glom}, based on an iterative "Unfolding" algorithm. By making an empirically derived assumption about the shape of the particles (glomeruli) in the model, we calculate the distribution of profiles that would arise from randomly sectioning a particle given its size. Importantly, the largest observed profiles must come from the center of the largest particles. We thus "unfold" the histogram by iteratively counting the largest particles and then subtracting the smaller profiles from the distribution that would result from sectioning those particles. To apply and

test the Unfolding algorithm, we first simulated a set of glomerulus profiles and compared the calculated glomerulus radii to the original “true” simulated radii. Then we repeated this comparison using ellipsoidal, rather than spherical, simulated particles. Next we applied this technique to examine the distribution of IV_{glom} in oligosyndactyl (Os/$^{+}$) mice, a model of kidney pathology that exhibits reduced nephron number by nearly 50% and glomerular hypertrophy compared to wild type (WT) controls (16). By examining a large population of glomerulus profiles, we elucidated differences in numerical and spatial distributions of hypertrophic glomeruli. We hypothesized that Unfolding enables accurate measurements of heterogenous glomerular morphology in individual kidneys.

Chapter 1 – Development and validation of the Unfolding model

The goal of this work is to develop a stereological method to measure the number, average volume, and distribution of volumes of glomeruli in the mouse kidney. While other methods may be used to determine the number and average volume of glomeruli, they cannot estimate the distribution of volumes. We approached this problem using the Unfolding concept, which was first proposed in 1925 by Wicksell(17), but has not been robustly validated or applied to the problem of counting glomeruli. In the first portion of this work, we will develop and validate the Unfolding algorithm.

The Chapter begins with a mathematical outline of two common methods for determining N_{glom} and AV_{glom}, followed by a formal description of the Unfolding model. The model is then validated by simulating a set of spherical glomeruli and a random set of profiles that might be obtained by sectioning that population of glomeruli. By convention the 3D spheres are called 'particles' and use upper-case variables, while the 2D slices are called 'profiles' and used lower-case variables. We then use the unfolding algorithm on the simulated profiles to recover the original distribution of particles. To measure the accuracy of the result, we routinely calculate the 'fidelity' of the algorithm, defined as the correlation coefficient between the known distribution of particle radii and that calculated by Unfolding. We test the algorithm given several different assumptions about the underlying distribution of particle Radii. Next we acknowledge the fallibility of a key assumption of the model—that glomeruli are spheres— and repeat the simulations using glomeruli that are ellipsoidal rather than spherical, without altering the model, to examine the detrimental effects on the result. Finally, we explore the conditions under which the model is valuable, considering the distribution of particle sizes, available number of samples, and homogeneity of particle shape.

General stereological model

Table 1. Summary of Variables

Description	Symbol	Expression
Total glomerular number	N_{glom}	$N_V V_{Cortex}$
Average glomerular volume	AV_{glom}	
Individual glomerular volume	IV_{glom}	$\frac{4}{3}\pi R_n^3$
Intra-renal standard deviation of glomerular volume	σ_{glom}	
Measured profile area	a_n	
Radius of a circle of equivalent area	r_n	$\sqrt{a_n/\pi}$
Slice thickness	t	
Radius of individual glomerulus	R_n	
Mean radius	R_0	
Number density per unit area	N_A	
Number density per unit volume	N_V	$N_A/2R_0$
Area density per unit area	A_A	
Volume density per unit area	V_V	A_A
Cortical volume	V_{Cortex}	

If a volume containing particles (such as glomeruli) is sectioned with a slice thickness much less than the size of the particles, the sections will contain a distribution of 2D profiles cut from those particles. For a collection of *N* spherical particles, each with radius R_n, in a cubic volume with side length *l*, the problem is to estimate the number and size of the particles from slices taken through the volume. By convention, capital *R* is used to indicate particle radius and lower-case *r* is used to indicate profile radius. All variables are summarized in Table 1. Taking an infinitely thin slice at a randomly chosen location through the box, the probability that the slice will intersect the n^{th} particle is

$$Pr\{n\} = \frac{2R_n}{l} \equiv \alpha_n, \tag{1}$$

where α_n, with values between 0 and 1, is the probability of detecting the n^{th} particle.

In a single thin section of tissue, the fraction of total area containing particles is denoted A_A. Similarly the fraction of the total volume containing particles is V_V. These two quantities are equal according to the Delesse Principle (7), therefore the total glomerular volume $V_T = V_V V_{Cortex}$. Since $V_T = N_{glom} A V_{glom}$, by accurately estimating either the number or average volume of particles, the other quantity may be calculated using

$$N_V = \frac{N_A}{2R_0} \tag{2}$$

and

$$N_{glom} = N_V V_{cortex}. \tag{3}$$

Estimation of AV_{glom} by Weibel-Gomez

The Weibel-Gomez technique relies on the assumption that particles are spheres with normally distributed radii. It is laid out in detail in Weibel-Gomez (1962)(7). Briefly, define a unitless constant $\beta = \frac{V}{s^{3/2}}$, where *V* is the volume of an object and *s* is the average cross-sectional area across every plane. For a sphere, $s = \frac{2}{3}\pi r^2$ and $V = \frac{4}{3}\pi r^3$, therefore $\beta \approx 1.38$. The number of convex particles per unit volume, N_V, can be calculated by $N_V = \frac{1}{\beta_i}\sqrt{\frac{{N_A}^3}{V_V}}$. N_A and V_V can both be measured by unbiased stereological methods, however, this equation still assumes that all particles are the same size. Since larger particles are more likely to be sampled, the above measurement will systematically underestimate the number of particles. Therefore a second constant, *K*, is defined as the ratio of the skewness of the distribution of radii to the mean radius, and has been experimentally estimated to be ~1.04(18). Therefore the final equation for estimating number density is $N_V = \frac{K}{\beta_i}\sqrt{\frac{{N_A}^3}{V_V}}$. Given N_A, V_{glom} and N_{glom} can be estimated using equations 2 and 3.

Estimation of N_{glom} by Fractionator Dissector

The Fractionator-Dissector technique for determining N_{glom} is an unbiased technique that doesn't rely on an assumption of particle size or shape. The basis of this technique observing two imaging planes of the same tissue separated by a known distance, dS. This can practically be accomplished by taking two physical sections and aligning them physically(19) or by using a confocal microscope to collect optical sections at two different depths(20). Next the number of nephrons that appear in one, but not both, sections is determined. By using this trick the probability of detecting the n^{th} particle $P\{n\} = 2dS/l$, crucially not depending on the size of the particle. Therefore Equation 3 can be used to calculate an unbiased N_{glom} where $N_V = {counts}/{A_{cortex}dS}$.

Estimation of AV_{glom} and distribution of IV_{glom} by Unfolding

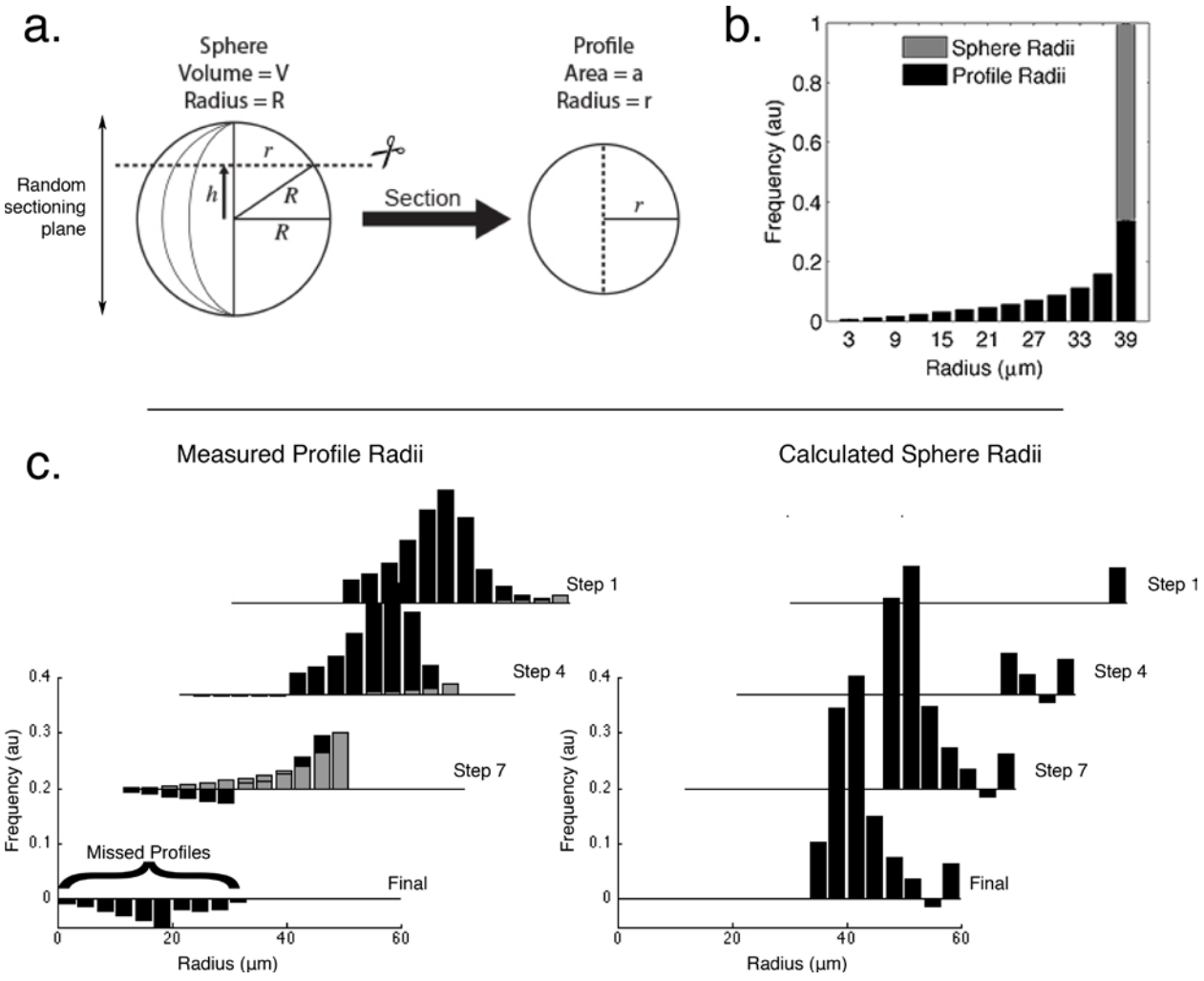

Figure 1. (a) A sphere with radius R cut by sampling planes at a random height (h) will produce a distribution of profiles, each with radius r. (b) The distribution of profile radii expected from randomly slicing a sphere of r=39μm. Since the measured data is a collection of profiles cut from spheres of different sizes, we developed an Unfolding

algorithm to estimate the original distribution of spheres from the collection of observed profiles. (c) The Unfolding procedure is based on the principal that the largest profiles are sections cut from the center of the largest population of spheres. Beginning with the largest size class, we calculate the number of spheres (bottom right) of that radius that produce the observed number of large profiles. Next we subtract all of the profiles that would arise from those spheres from the histogram (shown in gray, bottom left). This process is repeated until all the observed profiles are accounted for.

Box 1: Derivation of Equation 2

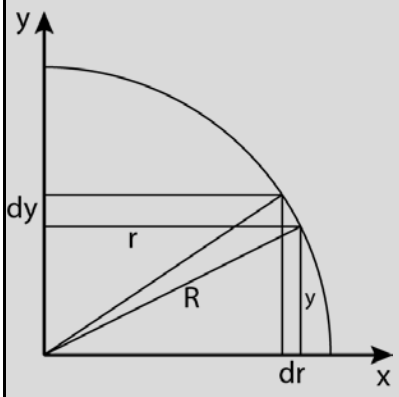

From the Pythagorean theorem

$$y(r) = \sqrt{R^2 - r^2}$$

Whose derivative is

$$\frac{dy}{dr} = \frac{1}{2}(R^2 - r^2)^{-\frac{1}{2}}(-2r) = \frac{-r}{\sqrt{R^2 - r^2}}.$$

Since the height through which a glomerulus is cut *y*, is a uniform random variable, if y_i is between *y* and *y+dy*, then r_i is between *r* and *r-dr*:

$$\Pr\{r < r_i < r - dr|R\} = dy/R.$$

By substitution, the continuous probability distribution function is:

$$\phi(r|R)dr = \frac{-r}{R\sqrt{R^2 - r^2}}dr.$$

The discretized version of the function gives the probability that r is between r_n and $r_n - \Delta r$ where r_n is the upper bound of the n[th] bin and Δr is the bin width

$$\Pr\{r_n|R\} = \int_{r_n - \Delta r}^{r_n} \phi(r|R)dr = \frac{\sqrt{R^2 - r^2}}{R}\Bigg|_{r_n - \Delta r}^{r_n}$$

If a single sphere with radius *R* is intersected by a slice at a uniformly randomly distributed location, the probability density of observing a profile with radius *r* in the slice is

$$\psi(r|R)dr = \begin{cases} \dfrac{r}{R\sqrt{R^2 - r^2}}dr, & r < R \\ 0, & r \geq R \end{cases} \quad (4)$$

(Figure 1a) (21). Equation 4 is illustrated in Figure 1b. We adopt the convention that a single slice through the volume can intersect with each particle only once. If the slice does not intersect with the n^{th} particle, the observed radius will be 0. These observed profiles with r=0 are represented by a delta function $\delta(r)$ that satisfies $\int_{-\infty}^{\infty} \delta(r)dr = 1$. From Equation 1, the total probability distribution function (PDF) is the sum of these two functions weighted by the probability of detecting (α_n) or not detecting ($1 - \alpha_n$) the n^{th} glomerulus. Because the glomeruli are small and sparse, we assumed that the excluded volume effect was negligible. Therefore the expected distribution of profile radii in a slice through a control volume containing *N* particles each with a radius of R_n will be:

$$Pr(r)dr = \frac{1}{N}\sum_{n=1}^{N}\left(\alpha_n \frac{r}{R_n\sqrt{{R_n}^2 - r^2}}dr + (1 - \alpha_n)\delta(r)dr\right). \quad (5)$$

Pr(r) is the probability that the n^{th} particle will be detected as a profile of radius *r* in a random slice. Because the location of the n^{th} particle is unknown, the slice may not intersect the particle. This case yields an observed radius of 0 for that particle, represented by the second term inside the parentheses. If the slice intersects the n^{th} particle, with probability α_n, the profile radius depends on the particle radius as in Eqn. 2. However, because the particle radius is also unknown, the PDF is averaged over all particles in the volume. Each section results in one measurement of the profile (which may be 0). Thus the equation sums to 1. Because the unobserved profiles with r=0 cannot be measured, we must estimate the number of unobserved profiles from those that were observed. (Equation 2b formally describes the probability of detecting a profile of a specific radius, but the formula used in the algorithm is given in Eqn 6.)

Methods

Volume Distribution by Unfolding

To estimate the distribution of true glomerular radii R_n from the measured profile radii r_n, we developed and applied the Unfolding algorithm based on the theory described by Wicksell in 1925(17). We first sorted the measured r_n into a normalized histogram of 18 bins evenly spaced from 0 to 60μm. The number of bins should depend on the number of observations and the variance but will generally fall between 16 and 20 for this procedure(21). We assumed that the profiles in the largest bin of this histogram arose from sections near center of the largest glomeruli. We also assumed that there were no particles larger than the largest observed profile. To find the probability that an observed profile will have a radius between r_m and r_m- Δr we discretized Eqn. 4:

$$\Pr\{r_m|R\} = \int_{r_m-\Delta r}^{r_m} \psi(r|R)dr = \frac{\sqrt{R^2 - r^2}}{R}\Bigg|_{r_m-\Delta r}^{r_m} \tag{6}$$

where r_m is the upper bound of the m^{th} bin and Δr is the bin width. Next, beginning with the bin of largest profiles, we calculated the fraction of glomeruli with the corresponding radius and the expected number of profiles in each smaller profile bin attributed to glomeruli in this size class. We removed these calculated values of *r* from the histogram and repeated the process for the bin of next largest profiles. The bins with negative frequency, after all expected profiles were subtracted, represented profiles from larger glomeruli that were not identified due to experimental challenges. Frequencies in the final histogram were corrected by a factor of R_n/R_0 to account for the increased likelihood of observing larger glomeruli explained by Eq 1. Finally, we calculated the average radius R_0 from the histograms. V_{cortex} was measured directly from the 3D MR images, and N_{glom} and AV_{glom} were calculated according to Equation 3 and $AV_{glom} = \frac{4}{3}\pi R_0^3$. For reproducibility, the MATLAB code has been included as supplemental material.

Unfolding validation

To test the Unfolding algorithm, we simulated the kidney as a cube filled with 10,000 spherical glomeruli uniformly distributed inside. In the simulated samples the radii were normally distributed (37±3μm) (Figure 2, left) or bimodally distributed (70% 32±3μm, 30% 45±3μm, Figure 2, right), which was approximately the range of glomerular radii measured here. (The mean glomerular radii of Os/$^{+}$ and WT mice were 44±1.4μm and 36±1.7μm respectively). Next we simulated the profile radii that would be expected if seven uniformly spaced, infinitely thin, sections were taken through the volume, and calculated the particle radii from the distribution of these observed profile radii using the Unfolding algorithm. Finally we computed the correlation coefficient between the original distribution of particle radii and the distribution of particle radii calculated from the Unfolding algorithm. We defined this correlation as "fidelity". To assess this, we performed the same simulation 1000 times using normal and bimodal distributions of particle radii. To test the sensitivity of Unfolding to the standard deviation of the particle radius distribution, we performed the simulation for particles with normally distributed radii 1000 times while varying the standard deviation from 0 to 5μm— a conservative estimate of σ_{glom} (Figure 2, insert). Because the unfolding algorithm is applied serially, errors might be systematically propagated across histogram bins. To assess the magnitude of this effect, we examined the correlation between the number of profiles in the bins containing the largest profiles and the fidelity of Unfolding. To assess the effect of measurement error on the algorithm, we introduced artificial measurement error (0-25%) and repeated the simulations. We chose this range because, in our experience, typical inter-investigator variability is ~5-10%. Finally, we ran the simulations a number of times using different values of AV_{glom}, σ_{glom}, and distributions of IV_{glom}, estimating the minimum number of profiles that must be sampled for the Unfolding algorithm to have an average fidelity of 90%. The results are not shown, but the estimates are given in the discussion as a guideline for using the Unfolding algorithm in other species.

To test how the assumption of spherical glomeruli affects the accuracy of Unfolding and estimates of N_{glom} and AV_{glom}, we simulated profiles cut from a triaxial ellipsoid defined by two axial ratios and a volume. We generated triaxial ellipsoids in MATLAB with equivalent volumes to the spheres used in the first set of simulations (2.12±0.51 x10^{-4} mm^3). The ratio of the lengths of the second and third axes, with respect to the shortest axis, was uniformly distributed between 1 and 1.63. To choose the maximum possible axial ratio (1.63), we varied that parameter from 1 to 2, and selected the value that produced an average 2D profile axial ratio of 1.26 (the glomerular axial ratio that was observed in this work). Next, we found the area of the 2D ellipse formed by the intersection of each 3D ellipsoid and a plane passing in uniformly distributed random orientation through the ellipsoid according to the method of Klein(22). While still assuming the particles were spheres, we repeated the Unfolding procedure 1000 times and compared the estimated sphere volumes with the known ellipsoid volumes.

Parameter optimization

To estimate the number of samples required for the Unfolding method to be viable, we examined several different scenarios, each assuming a different distribution of particle sizes, then simulated

corresponding sets of particles and profiles. Next, we used the unfolding algorithm with a variable number of sampled profiles and examined the average (n=1000 runs) correlation coefficient between true distribution and that calculated by unfolding. We report the smallest number of samples required for an average correlation coefficient of 0.90.

The effect of bin size on fidelity is necessarily intertwined with the number of profiles sampled. More bins requires more samples to reduce sampling noise. Therefore we repeated the simulation on normally distributed simulated particles (37±3μm) as before and varied the number of samples from 500 to 2000 and the number of bins from 16 to 40. We calculated the average (n=2000 runs) correlation coefficient between true distribution and that calculated by unfolding.

Results

Validation of the Unfolding algorithm

To test the accuracy of the Unfolding algorithm, we used a simulated data set consisting of random populations of spherical particles, (as a model for glomeruli), and the corresponding circular profiles of these particles observed by randomly sectioning the 3D volume. The intra-renal distribution of IV_{glom} was calculated from profile radii for particles of normally distributed size, shown in Figure 2. The correlation coefficient between the calculated and true radii was 0.96 for normally distributed radii and 0.95 for bimodally distributed radii. Increasing the standard deviation of particle radii in the simulation to 5 μm decreased the correlation coefficient slightly to 0.95 (Figure 2, insert).

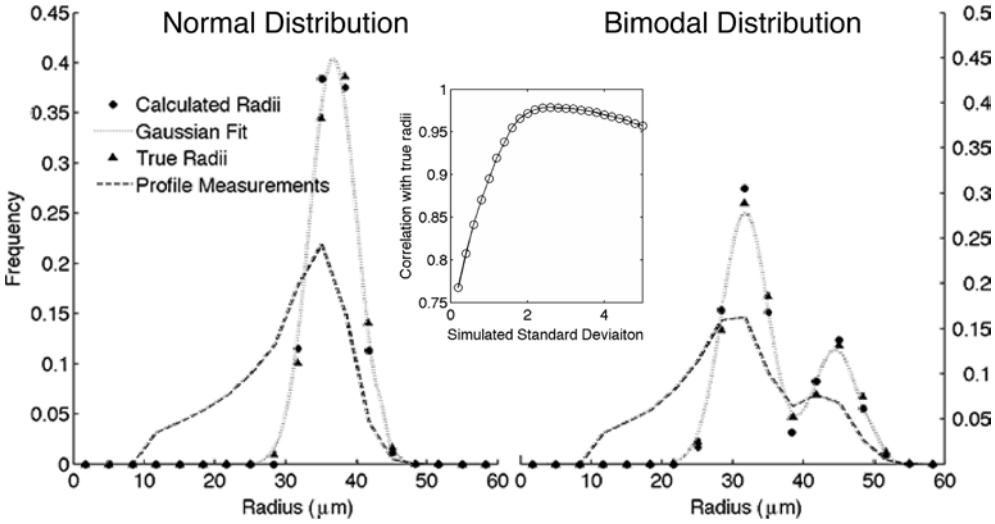

Figure 2. An Unfolding algorithm was developed to calculate the true radii of glomeruli from measured profiles. Here, the algorithm was validated using simulated data based on normally distributed spheres (left) or bimodally distributed spheres (right). We calculated the correlation coefficient between the known simulated particle radii and the calculated particle radii; the algorithm was accurate even with a broad distribution of particle radii (insert).

To determine the importance of error caused by assuming that glomeruli are spherical, we simulated the case in which glomeruli are triaxial ellipsoids. We based the shape on our experimental findings, where the mean ratio of the major and minor axes of the measured glomerular profiles was 1.26±0.03 in Os/$^{+}$ and WT mice (with no difference between genotypes). In

the model, this corresponded to a set of ellipsoids in which the length of shortest axis was *a*, and the other two axes were *b*a* and *c*a*, where *b* and *c* were uniformly distributed values between 1 and 1.63. When we used the Unfolding algorithm to estimate the volumes of these triaxial ellipsoids from random profiles, the correlation coefficient between the histograms of the calculated and true volumes was 0.88, and AV_{glom} was underestimated by 3.6% on average. To test the fidelity of Unfolding in the presence of measurement error, we repeated simulations with artificial error of 0-25% of the profile radius. Measurement error below ±15% decreased the fidelity ~2-3%; ±25% measurement error decreased fidelity to ~85%. We estimate that typical inter-investigator variability is ~5-10%. To test the robustness of the Unfolding algorithm to sampling error, we examined the simulations with an unusually large or small frequency of profiles in the bins containing the largest profiles. We found no correlation (r^2~10^{-4}) between the frequency of the largest profiles and the fidelity of the algorithm.

Estimating the required number of samples

We extended our computer simulations to estimate the number of profiles per kidney that must be sampled for the Unfolding algorithm to be accurate, (defined by at least a 90% correlation with the true distribution). In general, the number of samples depends on the expected distribution of glomerular (particle) radii. Regardless of the number of profiles needed for accurate Unfolding, uniform random sampling with good spatial coverage is required for an accurate estimate of N_{glom}. The following guidelines are based on calculations in our laboratory (data not shown): For normally distributed glomerular radii with R=100±5μm, 300 profiles are sufficient. If the standard deviation is increased to 20μm, then 700 profiles are required. If a second population of larger glomeruli is present, e.g. a bimodal distribution where 80% of radii are 100±5μm and 20% are 125±5μm, 500 profiles are necessary. If the second population is smaller than the median, e.g. a bimodal distribution where 80% of radii are 100±5μm and 20% are 75±5μm, only 400 profiles are necessary. This is because larger glomeruli are more likely to be sampled, so a second population of large glomeruli biases the distribution more than a second population of small ones. For a trimodal distribution, e.g. 75±5μm, 100±5μm, and 125±5μm radii in a 10/80/10 ratio, ~500 profiles are needed. For reference, ~75 profiles were observed in a single axial section of a mouse kidney. Regardless of the required total number of profiles, uniform random sampling procedures must be observed. These estimates are meant to serve as a guideline rather than a precise number, and preliminary data should be used to gauge the expected distribution.

Effect of bin size

To examine the effect of bin numbers, we repeated the simulations examining the fidelity of the algorithm with different numbers of bins between 0 and 60μm. Increasing the number of bins increases the resolution of the histogram and therefore naturally should require more sampled profiles. Figure 3 shows the fidelity of the algorithm for different combinations of number of bins and number of samples.

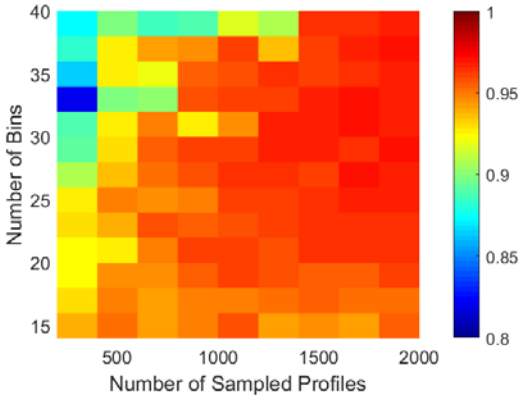

Figure 3. Effect of number of bins and number of samples on fidelity of the Unfolding algorithm. Color indicates the correlation coefficient between the known histogram and that calculated using the unfolding algorithm.

Discussion

In this chapter, we present a model-based stereological approach to measure intra-renal distribution of IV_{glom}. While other stereological techniques exist for estimating N_{glom} and AV_{glom}, they cannot be used to estimate the distribution of IV_{glom}. We tested the ability of the Unfolding technique to recover the distribution of particles from a set of profile measurements by simulating spherical profiles with a known volume distribution; the correlation between the known and calculated distribution was 96%. Next we tested the algorithm using simulated profiles cut from random triaxial ellipsoids rather than spheres. The correlation between the true and calculated volume distribution was 88% and AV_{glom} was underestimated by 4%. We considered a number of potential distributions of glomerular volume and estimated the number of samples required for the unfolding algorithm to be valid. A conservative estimation for mouse glomeruli is to expect a bimodal distribution with the second population of glomeruli being fewer and larger than the first. Therefore our calculations suggest we need at least 500 sampled profiles. Since our experimental design gave us at 700 samples per kidney, bin number should be between 18 and 26 (evenly distributed between 0 and 60μm. In conclusion, the Unfolding algorithm is useful for calculating N_{glom}, AV_{glom}, and the distribution of IV_{glom} in mouse kidneys.

Alternate applications of the Unfolding algorithm

Stereology has several biological applications, such as measuring the endowment of cells or vessels, and non-biological applications, such as analyzing sediment in rocks. Ideally the Unfolding algorithm would be applied to multiple problems in which the distribution of particle sizes is useful. This iteration of the Unfolding algorithm relies on the assumption that glomeruli are spherical, and the algorithm could readily be applied to any stereological application where sphere counting is required. More fundamentally, Unfolding requires only that particles be consistently shaped, so that all particles can be described by a single characteristic measurement of particle size (in this case Radius). To extend Unfolding to non-spheres, one must derive an equation akin to Equation 4 that describes the probability distribution of areas of random profiles as a function of the characteristic size of the particle. That equation could be the sum of multiple PDF describing a mixed population

of particles. Since spheres have rotational symmetry in 3 dimensions, Equation 4 was easily derived. While these PDFs have been determined for other ideal shapes(7), simulation may be necessary to solve more complex shapes(23). Some applications that meet these requirements include cell counting (for example podocytes, hepatocytes, or neurons), bubble counting (in solutions, suspensions like concrete, or against material surfaces), or sediment analysis.

Chapter 2- Demonstration of Unfolding in WT and Oligosyncactyl mice

In the first portion of this work, we developed an algorithm for calculating the distribution of particle volumes from a collection of thinly sliced profiles. We validated the assumptions considering the shape of mouse glomeruli, number of possible profile samples, and distribution of glomerular volumes. In this Chapter we will apply the Unfolding algorithm to compare the distribution of glomerular volumes in wild type (WT) and oligosyndactly (Os/$^{+}$) mice. The Os/$^{+}$ strain exhibits ~50% reduced kidney mass. We first use the unfolding algorithm to compare the distribution of IV_{glom} for WT and Os/$^{+}$ mice. Next, as a secondary method of validating the Unfolding algorithm, we compare the values of N_{glom} and AV_{glom} estimated by Unfolding to those estimated by Weibel-Gomez and by MRI. Finally, we examine the location of the largest glomeruli in both strains of mice. We hypothesize that the Unfolding algorithm will give new insight into the morphological changes in the whole population of glomeruli that are associated with reduced kidney mass.

Methods

Animal model

All animal experiments were approved by the Institutional Animal Care and Use Committee at University of Virginia and performed according to the NIH Guide for the Care and Use of Laboratory Animals. Five Os/$^{+}$ and five WT mice were used for the study. One Os/$^{+}$ mouse was later removed from the study as outlier. The mice were bred in-house on a predominately C57Bl/6 background. The Os/$^{+}$ mice were identified by syndactylism of the toes (15).

Tissue preparation

Mouse kidneys were fixed by perfusion using 0.9% sodium chloride followed by 10% neutral buffered formalin and stored in 2% gluteraldehyde in 0.1M cacodylate buffer at 4°C. To achieve histology blocks suitable for sectioning, the kidneys were embedded in gelatin (300 Bloom, 15% gelatin in PBS). These were crosslinked overnight with formalin at 4°C. The kidneys were exhaustively sectioned at a nominal thickness of 75 µm using a Leica VT1000S vibrating microtome. Every 8th section, beginning with a random section was selected for imaging. (e.g. Beginning with section number 3,11,19, etc., where 3 was the first section chosen using a random number generator). Freshly cut floating sections were blocked with 2% BSA, 1% Triton X-100 for 1 hour at room temperature with gentle shaking, then stained with 1 µg/ml wheat germ agglutinin-Alexa-555 (WGA-555) conjugate in PBS with 0.1% BSA overnight at 4°C, then washed 3x for 15 minutes with PBS. WGA-555 binds to sialic acids and N-acetylglucosamine on the surface of podocytes(24). It was used to highlight glomeruli at an imaging wavelength where there is little tissue auto-fluorescence. The sections were wet-mounted with ProLong Diamond (Life Technologies), covered with #1 glass coverslips, and sealed after 24 hours.

Confocal imaging and measurements

3D images were acquired on a Zeiss LSM710 confocal microscope running Zen 2012 software. A 561nm laser line excited the Alexa-555 fluorophore and Zen selected the emission filter

automatically (566-697nm). Z-stacks of tiles with 0.83x0.83x2.0μm resolution were collected at10μm intervals in Z. Since the microscope field of view is much smaller than the slice of tissue, multiple images were collected in a tiling scheme. A complete raw image of one slice of kidney might consist of 10x20x6 different individual images. The tiles were stitched in the XY plane using the 'Stitch' function in Zen.

To correct for tilted or wrinkled tissue slices, a smoothing operation was developed in MATLAB (MathWorks, Matick MA). The goal of this algorithm was to combine data from multiple focal planes to form a single image that is always in focus. This was accomplished by first finding the brightest pixel in Z at every point. Next that matrix of indexes was blurred with a Gaussian lowpass filter (size = 200, standard deviation = 50) using the imfilter function in MATLAB. Finally, the smoothing operation selected the brightest xy region out of all z-slices and then returned a single composite image of the brightest regions acquired.

Glomeruli were clearly identifiable compared to the background tissue (Figure 5). An average of 705 glomeruli per kidney were identified manually to the edge of the capillary tuft. Segmented mask images were generated in FEI Amira 5.6.0 software (Hillsboro, OR, USA). (This segmentation could easily be performed in many other image processing software packages).

Estimation of AV_{glom} and N_{glom} by Weibel-Gomez

The Weibel-Gomez technique assumes that glomeruli are spheres in estimating AV_{glom} and N_{glom}. The technique is based on Eqn. 1 and uses constants k and β to correct for the size distribution and shape of the glomeruli respectively, and glomerular area density per kidney unit area A_A.

$$N_v = \frac{k}{\beta}\sqrt{\frac{{N_A}^3}{A_A}}. \tag{7}$$

Previously reported values for k and β are 1.04 and 1.38 respectively(18). N_A is the number of profiles per unit area of cortex and A_A is the glomerular area per unit area of cortex. Here N_{glom} was calculated according to Eqn 3. To calculate AV_{glom}, we set the volume fraction of glomeruli, $V_V = A_A$ (Delesse principle) and used the formula:

$$AV_{glom} = \frac{V_V V_{Cortex}}{N_{glom}}. \tag{8}$$

Measurement of AV_{glom} and N_{glom} by MRI

We compared the AV_{glom} and N_{glom} obtained by Unfolding to those obtained by MRI of the same kidneys. The MRI techniques are described in previous work(11,14,25). Briefly, the mice were given a total of 5.75 mg/kg cationized ferritin (Sigma Aldrich, St. Louis MO) by retro-orbital injection in two doses spaced 1.5 hours apart. 1.5 hours after the last injection the mice were sacrificed by CO_2. Blood was removed by transcardial perfusion with 0.9 M NaCl and stored in 2% gluteraldehyde/0.1 M cacodylate buffer at 4°C. MRI was performed on a Bruker 7T/30 MRI (Billerica, MA), TE/TR = 20/80ms, resolution=50x50x55μm.

To measure N_{glom} and AV_{glom}, we developed an image-processing algorithm in MATLAB. Local minima in the images were identified using a watershed algorithm, and individual glomeruli were counted if their component pixels were connected within a specified radius of 26 pixels. Next we isolated a line profile of 11 pixels in each direction (x-axis) of the center of the glomerulus, and measured the width of the artifact at 55% of the maximum depth. This width was chosen because it produced the same AV_{glom} as Weibel-Gomez stereology.

Location of largest glomeruli

We noted in manual inspection of the image slices that larger glomerulus profiles were more frequently present in the juxtamedullary region than in the cortex. Because the sagittal tissue sections were randomly selected, the locations of glomeruli could not be directly compared between samples. Therefore, to determine if larger glomeruli were juxtamedullary, we collected coronal sections from the center of WT (n=3) and Os/$^{+}$ (n=3) kidneys (minimum of 74 profiles per kidney). Next we calculated the distance between each glomerular profile center and the nearest edge of the kidney section. We compared the average distance for the largest 10% of profiles to the average distance of all profiles in that kidney. Results shown are the average plus or minus the inter-mouse standard deviation.

Statistics

A Student's t-test was used to compare pairs of samples between groups. For multiple comparisons, one-way-ANOVA tests were performed in MATLAB using the 'multcompare' function. A p-value < 0.05 was considered significant.

Results

Tissue smoothing and segmentation

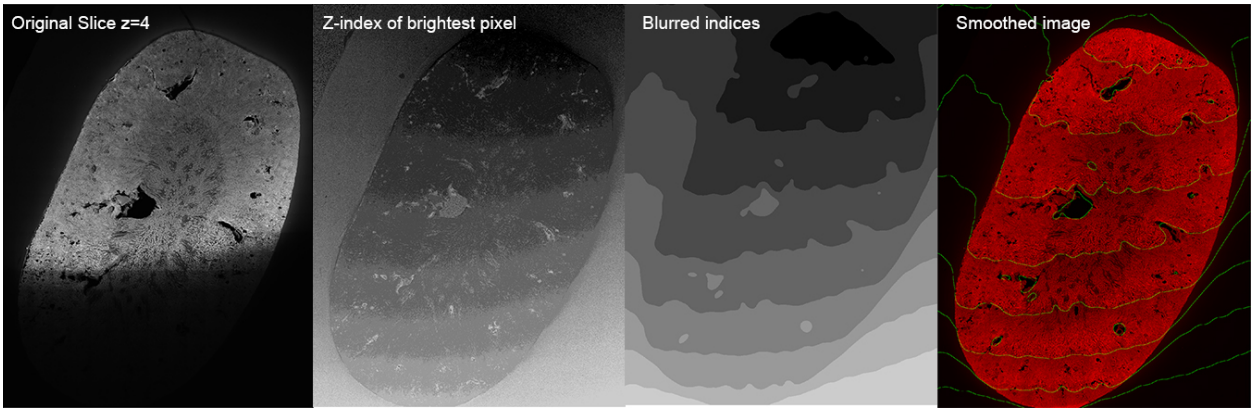

Figure 4. Visual representation of the smoothing algorithm designed to correct tissue mounting artifacts. Images from different focal planes are stitched together selecting regions of brightest signal intensity to ensure complete imaging of a surface that is not parallel to the slide. (first pane) One slice from the middle of the original 3D image stack. (second pane) z-location of the brightest pixel at every point in xy of the image. (third pane) a Gaussian blur applied to the previous image to regionally identify the brightest slice. (final pane) The smoothed composite image, green lines indicate the region boundaries. Please see Methods for detailed description of the algorithm.

The imaging plane of a confocal microscopes is always parallel to the slide, however tissue does not necessarily sit perfectly parallel to the slide due to imperfections in mounting. To produce single images suitable for manual segmentation, we developed an algorithm that regionally identifies the

brightest section in Z, then produces a single image. Figure 4 shows a tissue section that exemplifies the correction of a 'tilting' mounting artifact. Figure 5 shows the corrected image and the manually segmented map that was used as the raw data source.

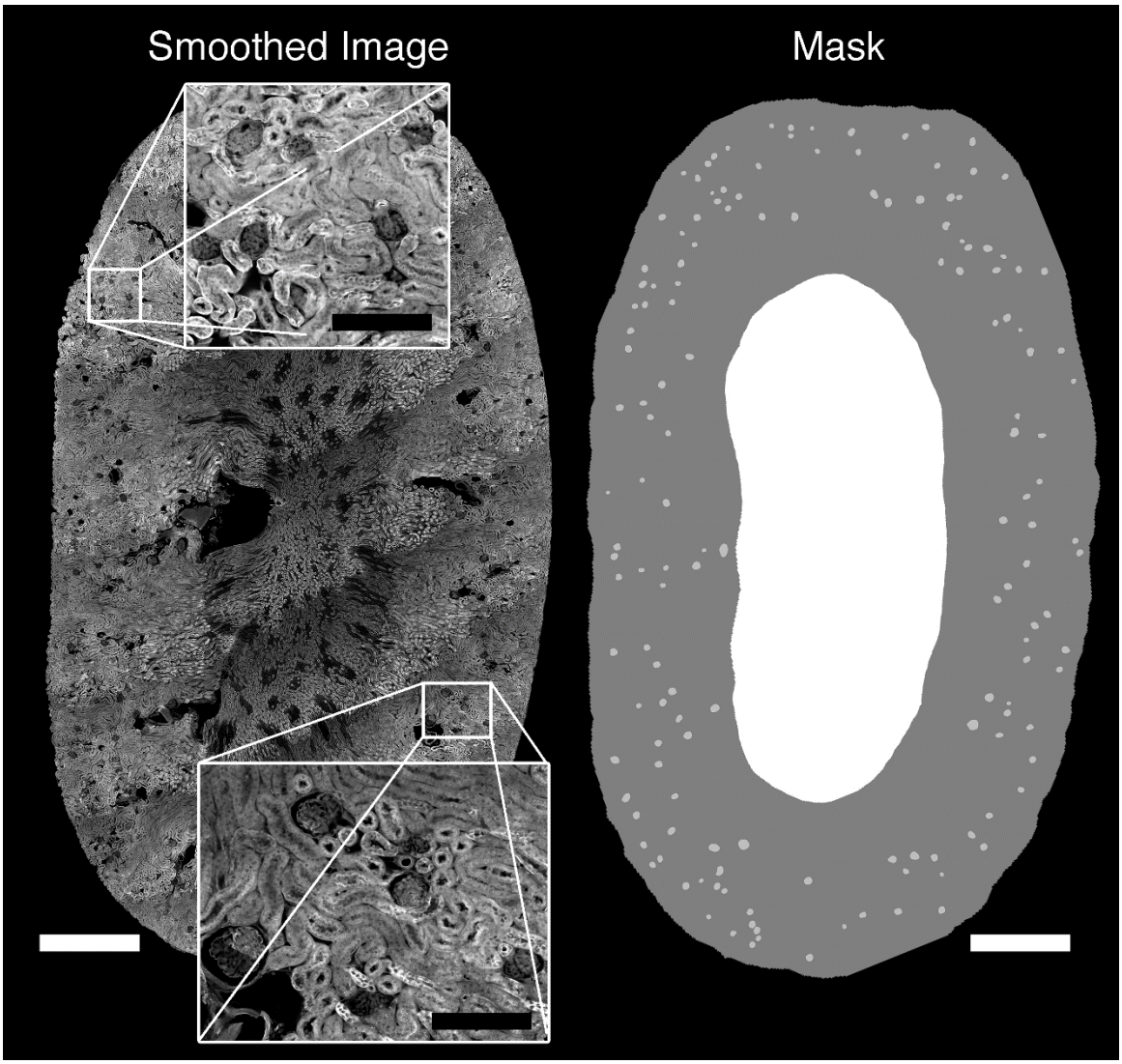

Figure 5. (left) Sample microscopy image after smoothing, showing full resolution detail in the inserts, scale bars are 1mm (white) and 0.2mm (black). (right) masks showing the segmented medulla, cortex, and glomeruli.

AV_{glom}, N_{glom}, and IV_{glom} distribution

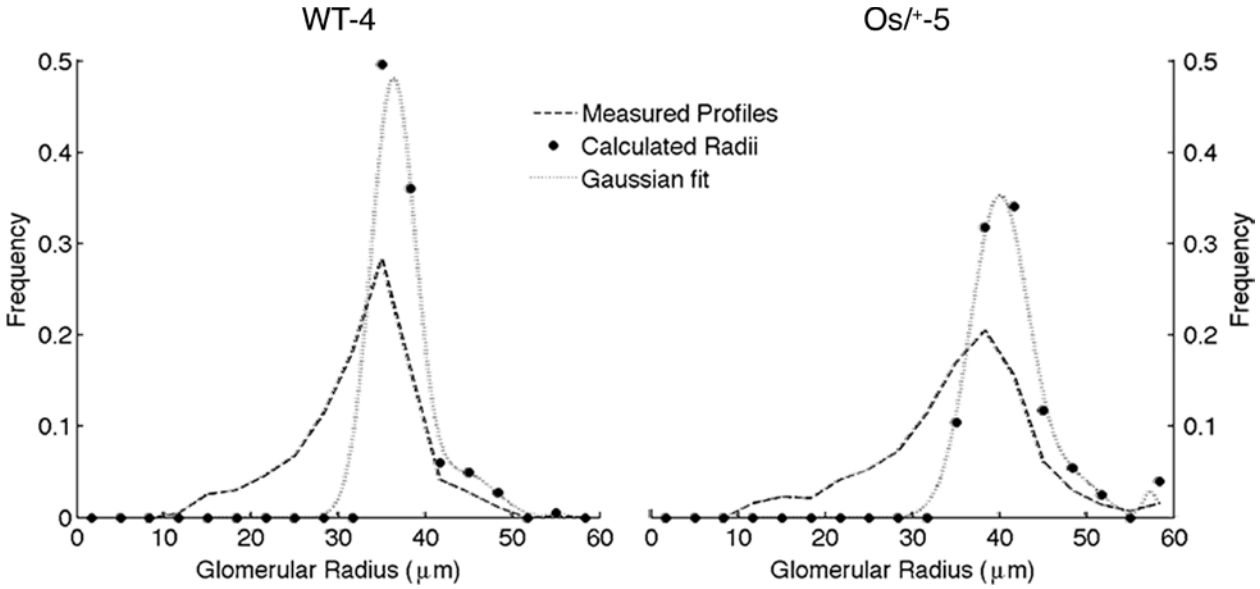

Figure 6. Unfolding of measured glomerular profiles for wild type (left) and Os/+ (right) mice. Dashed line indicates original distribution of the measured profile radii. Small profiles were observed less frequently than expected based on the profiles.

Glomeruli were traced manually from the confocal images. A sample image is shown in Figure 6. Sample histograms, fits of measured glomerular profiles, and calculated glomerular volumes are shown in Figure 4. AV_{glom} and σ_{glom} for each mouse were calculated from the distributions of IV_{glom} according to Eqn. 5 (Table 2). AV_{glom} was 2.01±0.28 x10^{-4} mm^3 for the WT mice (n=5) and 3.47±0.35 x10^{-4} mm^3 for the Os/$^+$ mice (n=4). The intra-sample volume standard deviation, σ_{glom}, was significantly larger for Os/$^+$ mice (1.4±0.19 x10^{-4} mm^3) than for WT mice (0.85±0.28 x10^{-4} mm^3). N_{glom} was estimated according to Eqn. 2. N_{glom} was 12,126±1658 (glomeruli/kidney) in the WT mice and 5,516±899 in the Os/$^+$ mice. In summary, the Os/$^+$ mice had 54% fewer ($p<0.001$) and 73% larger ($p<0.001$) and glomeruli than the WT mice. Os/$^+$-3 was clearly an outlier, N_{glom} and AV_{glom} were similar to the WT mice, and was omitted from the population comparisons.

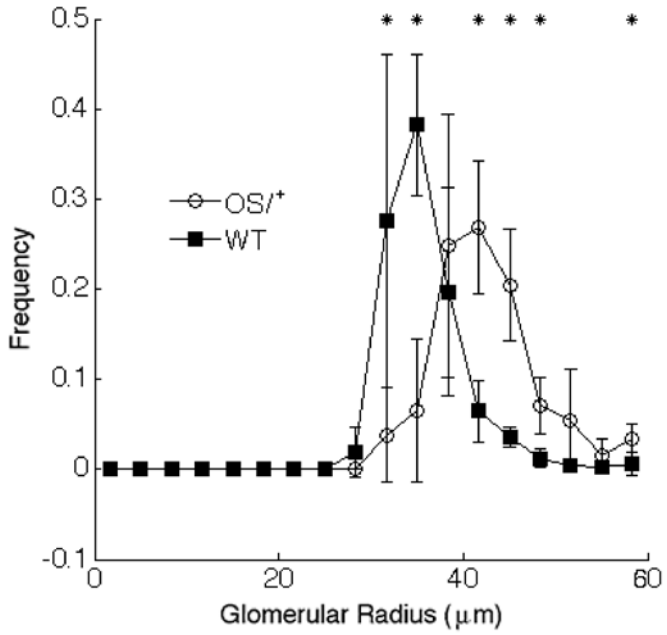

Figure 7. Comparison of the volume distributions of glomeruli in wild type (n=5) and Os/+ (n=4) mice. Error bars indicate inter-mouse standard deviation; stars indicate significant (p<0.05) differences between WT and Os/+ mice.

We compared the glomerulus volume distributions of the WT and Os/$^{+}$ mice, shown in Figure 7. The largest Os/$^{+}$ peak (3.0 x10^{-4} mm^3) was larger than the largest WT peak (1.8 x10^{-4} mm^3). The Os/$^{+}$ mice also had a larger standard deviation of intra-renal volume; σ_{glom} was 1.80±0.23 (x10^{-4} mm^3) in Os/$^{+}$ mice and 1.06±0.35 (x10^{-4} mm^3) in WT mice. Glomeruli in the largest size bin (r > 55μm) were observed significantly more frequently (p<0.05) in the Os/$^{+}$ mice (3.4±1.6%) than in the WT mice (0.6±1.2%). Thus Os/$^{+}$ mice had fewer, larger glomeruli with a broader intra-renal standard deviation.

Comparison with other methods

To validate the Unfolding algorithm as a predictor of N_{glom} and AV_{glom} we compared our results for the WT and Os/$^{+}$ glomerular endowment to estimates made with other stereological techniques (Table 2). There were no statistically significant differences in N_{glom} estimated by Unfolding or MRI. Others have found that the Weibel-Gomez overestimated AV_{glom} by 23% compared to the dissector method(26). In this work, the Weibel-Gomez estimate of AV_{glom} was 20% and 22% (for WT and Os/$^{+}$ mice) larger than that estimated by Unfolding, even when both numbers were calculated using the exact same data. This is because the Unfolding algorithm implicitly considers the undetected small profiles when determining AV_{glom}.

Table 2. To further validate the Unfolding protocol, we compared N_{glom} and AV_{glom} based on different stereological methods for the same kidneys. Unfolding, Weibel-Gomez, and MRI are based on the same samples (n=5). Unfolding and Weibel-Gomez are based on exactly the same data (images and segmentation).

Method	WT		Os/$^{+}$	
	N_{glom}	AV_{glom}	N_{glom}	AV_{glom}
Unfolding	12,126±1,658	2.01±0.28	5,116±899	3.47±0.35
Weibel-Gomez	11,600±1,009	2.41±0.23	4,723±640	4.24±0.30
MRI	12,529±703	2.68±0.11	5,126±689	3.18±0.39

Spatial distribution of the largest glomeruli

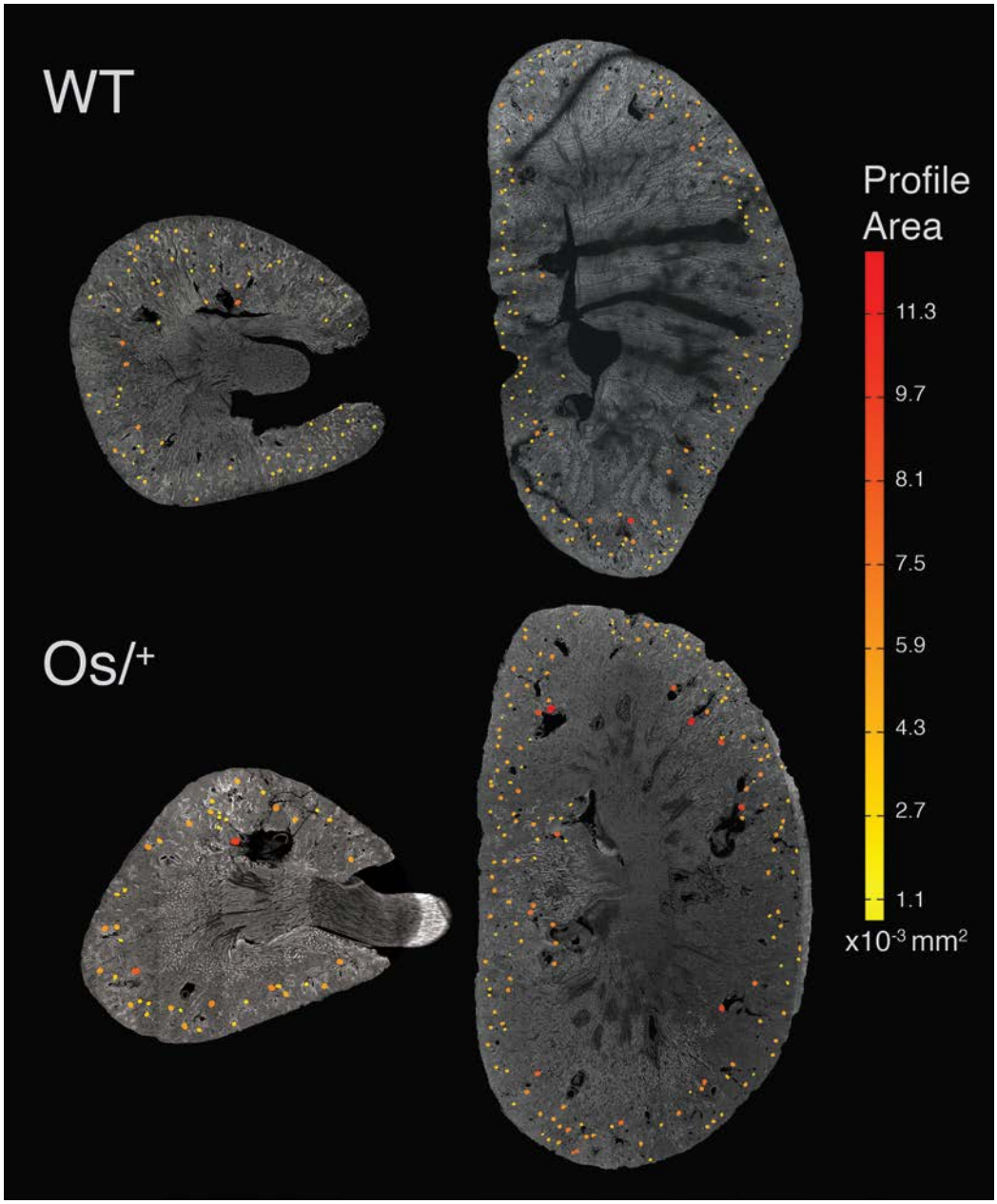

Figure 8. Overview of spatial distribution of glomeruli in representative wild type and Os/+ mice, mapped by glomerulus area. Color indicates the area of each measured glomerular profile. Larger glomeruli and increased frequency of glomeruli near large vessels were observed in the Os/+ mice. On average, larger glomerular profiles are found closer to the center of the kidney section.

Finally, we examined the spatial distribution of glomeruli based on their profile sizes, shown in Figure 8. For both WT and Os/+ mice, there were apparently three populations of glomeruli. The superficial glomeruli near the cortical surface were the smallest, the juxtamedullary glomeruli were visibly larger, and the glomeruli near major vessels were the largest. To verify this across all sections, we calculated the distance to the edge of the kidney section for every glomerulus (Figure 9). In the

WT kidneys the largest 10% of profiles were 1.12±0.26mm from the edge whereas all profiles were 0.59±0.12mm from the edge. In the Os/$^{+}$ kidneys the largest 10% of profiles were 0.82±0.14mm from the edge whereas all profiles were 0.46±0.14mm from the edge. The same trend was observed in sagittal sections of the kidney but was less pronounced. We did not compare between genotypes because WT kidneys are larger in general and the glomeruli should be farther from the edge of the kidney in WT mice. We conclude that larger glomeruli were on average located more deeply in the cortex.

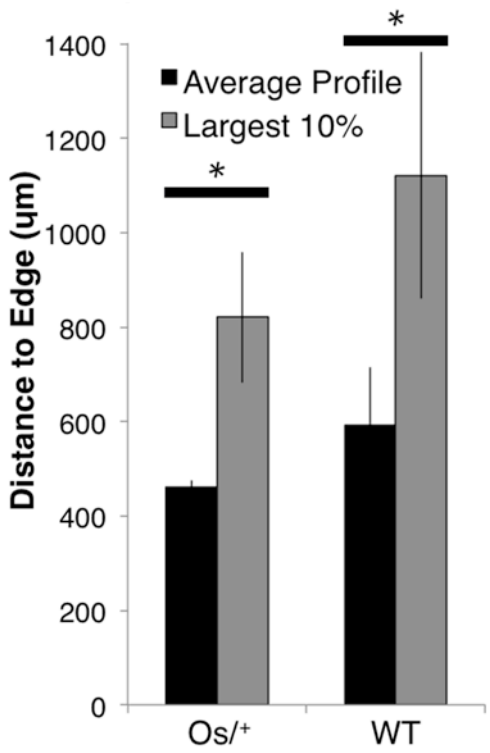

Figure 9. The average shortest distance to the edge of the coronal sections for all profiles compared to the largest 10% of profiles in WT (n=3) and Os/+ (n=3) mice. Asterisks (*) indicate statistically significant differences (p<0.05, t-test).

Discussion

In the second chapter of this work we applied the Unfolding algorithm to examine glomerular endowment in WT and Os/$^{+}$ mice; Os/$^{+}$ mice had 54% fewer glomeruli and 73% larger AV_{glom} than the WT mice. This is consistent with previous observations of the Os/$^{+}$ mouse(16). Finally we compared the estimate of N_{glom} by Unfolding to the estimates by MRI and Weibel-Gomez and found no significant difference between the different techniques. The measurements required for Unfolding are the same as those required for the dissector technique. Thus, the Unfolding approach could be used as a supplement to a design-based technique, calculating N_{glom} and AV_{glom} from the dissector method and distribution of IV_{glom} from Unfolding. If the geometry of the glomeruli is known, Unfolding may be used as a standalone approach. When we applied the Unfolding algorithm to WT and Os/$^{+}$ mouse models, we found that the Os/$^{+}$ had 54% fewer glomeruli and 73% larger AV_{glom} than the WT mice. This is consistent with previous observations of the Os/$^{+}$ mouse(16). Finally we

compared the estimate of N_{glom} by Unfolding to the estimates by MRI and Weibel-Gomez and found no significant difference between the different techniques. The measurements required for Unfolding are the same as those required for the dissector technique. Thus, the Unfolding approach could be used as a supplement to a design-based technique, calculating N_{glom} and AV_{glom} from the dissector method and distribution of IV_{glom} from Unfolding. If the geometry of the glomeruli is known, Unfolding may be used as a standalone approach.

Several sources of error and bias arise in measuring glomeruli from thin sections of kidneys. These include assumptions about size variance, shape, finite section thickness, ambiguity in identifying glomerular profiles, tissue preparation artifacts, and random sampling error. Bias due to variance in glomerular size arises from the fact that larger glomeruli are more likely to be sampled. This bias scales with $(\sigma/R_0)^2$, which is up to 4% for mouse glomeruli. This source of bias is easily corrected if σ_{glom} is determined. Bias from finite section thickness is due to the projection of a curved 3D profile onto a 2D imaging plane and scales with $\left(1 + {}^{3t}/_{2D}\right)^{-1}$; this was a ~4% overestimation of radius in this work (section thickness t = 2μm). Assuming the shape of glomeruli affects the estimations in two ways; it changes the probability of detecting a glomerulus (Eqn. 1) and causes underestimation of glomerular volume. If the profiles are considered ellipses rather than circles, the term R_n in Equation 1 must be converted to the mean caliper radius rather than the radius of a circle of equivalent area (measured here). The ratio between these is given by $\sqrt{\frac{1+q^2}{2q}}$ (21), where q is the axial ratio of the ellipse, and results in ~1.3% underestimation of N_{glom} for the axial ratio of 1.26 measured for glomeruli in this work. The effect of assuming shape on the unfolding algorithm is more complex. Here we underestimated the volume of non-spherical simulated data by 3.6%. However, more detailed studies of glomerular shape and shape distribution will improve the application of Unfolding. Ambiguity due to sampling error is particularly complex, because it depends on stain quality, imaging quality, tissue preparation, and researcher skill. In this work we identified almost no profiles with radius <20μm^2, which likely constitute up to 20% of possible profiles from the glomeruli. This is a systematic error in all stereological techniques. One can 'correct' the observed number of profiles to include this estimate of lost small profiles. However, because these small profiles are only assumed to exist, we chose not to make this correction here. Tissue shrinkage, another source of error, depends highly on the method of embedding and sectioning. Estimates range from 5-15% shrinkage for plastic embedding to 50% for paraffin embedding. Here we used a vibrating microtome to section fixed tissue(9). This alleviated the need to infiltrate the tissue with a hypertonic solvent (such as benzyl alcohol/paraffin, which causes tissue shrinkage), but required a confocal microscope be used to image the thick sections. Finally, based on the comparison between the MRI and stereology estimates of N_{glom}, we estimate ±5-10% sampling error when number of observations ~ 700. We conclude that systematic error and bias arising from tissue preparation, profile identification, and sampling may be much greater than the bias from size variance and assumptions about glomerulus shape.

All stereological techniques are biased from tissue preparation artifacts, small pieces of glomeruli that are lost during sectioning and finite section thickness. The dissector technique makes no assumptions about the size or shape of the glomeruli, however it can be subject to the tissue

processing artifacts and assumes unambiguously identified profiles. The Weibel-Gomez technique assumes the size variance and shape of glomeruli, but can be performed extremely quickly. Neither the dissector nor Weibel-Gomez techniques can be used alone to measure the distribution of IV_{glom}. Unfolding assumes glomeruli are spherical and is the only microscopy technique to determine the distribution of IV_{glom}. In this work, we used very thick (75μm) physical sections and confocal microscopy to obtain very thin optical sections (2μm), but standard light microscopy with Hematoxylin and Eosin staining would also be sufficient if thin (<5μm) sections were used. While the Unfolding technique introduces some bias, this bias is small compared to the error associated with tissue preparation, profile identification, and sampling error. Further, because large numbers of profiles are quickly identified and measured, the bias can easily be quantified and corrected.

In summary, Unfolding is extremely efficient, requires minimal equipment, produces results comparable to other stereological methods, and can be used to measure σ_{glom} and the intra-renal distribution of IV_{glom} (in addition to AV_{glom} and N_{glom}). In principle, Unfolding could be applied to measure intra-organ distributions of any number of structures. In the kidney, this could include vessel, podocyte and tubule diameters. Unfolding is thus a flexible technique that provides a new, quantitative view of morphology in the individual organ.

Conclusion

This work describes a novel stereological technique to measure intra-renal glomerular volume, applied to detect glomerular hypertrophy in the Os/$^{+}$ mouse model of low nephron endowment. The technique is based on an Unfolding algorithm applied to recover the original distribution of glomerular radii from a sample of profile measurements. In simulated data, the correlation between true and calculated particle radii was 96% accurate for Gaussian distributions and 95% accurate for bi-modal distributions of glomerular radii. When we made an alternate assumption— that particles are triaxial ellipsoids— the algorithm was 88% accurate and underestimated AV_{glom} by 3.6%. Comparing the volume distributions in Os/$^{+}$ and WT kidneys, we observed that the largest peak in the Os/$^{+}$ mice was shifted from the WT peak, and that glomeruli with a radius greater than 55μm were more prevalent. The Os/$^{+}$ mice had significantly fewer, larger glomeruli than the WT mice. Comparing several different means of estimation, (Unfolding, Weibel-Gomez, or MRI), we found no significant difference in estimates of N_{glom}. We conclude that the Unfolding algorithm is an efficient technique to measure the intra-renal glomerular volume distribution. This work may enable detailed studies of common kidney diseases that heterogeneously affect glomerular and nephron morphology.

Acknowledgements

The authors gratefully acknowledge A. Eggers and the lab of R. Gates at Hawaii Institute for Marine Biology and T. Carvalho and M. Dunlap at the Biological Electron Microscope Facility of the University of Hawaii for expertise in confocal imaging. We also thank Q. Liu and G. Turner at the Barrow Neurogical Institute-Arizona State University Center for Pre-Clinical Imaging. Finally, we gratefully acknowledge Daisuke Takagi at the University of Hawaii Department of Mathematics for reviewing the mathematics. This work was funded by NIH DK-091722 (KB) and The Hartwell Foundation(JC).

References

1. Hayman JM Jr, Halsted JA, Seyler LE. A comparison of the creatinine and urea clearance tests of kidney function. J Clin Invest. 1933;.

2. Nyengaard JR, Bendtsen TF. Glomerular number and size in relation to age, kidney weight, and body surface in normal man. Anat Rec. 1992 Feb;232(2):194–201.

3. Hinchliffe SA, Lynch MRJ, Sargent PH, Howard CV, van Velzen D. The effect of intrauterine growth retardation on the development of renal nephrons. BJOG: An International Journal of Obstetrics & Gynaecology. Blackwell Publishing Ltd; 1992 Apr 1;99(4):296–301.

4. Helal I, Fick-Brosnahan GM, Reed-Gitomer B, Schrier RW. Glomerular hyperfiltration: definitions, mechanisms and clinical implications. Nature Publishing Group. 2012 May;8(5):293–300.

5. Neuringer JR, Brenner BM. Glomerular hypertension: cause and consequence of renal injury. J Hypertens Suppl. 1992 Dec;10(7):S91–7.

6. Hoyer JR, Fogo AB, Terrell CH, Delaney MM. Immunomorphometric studies of proteinuria in individual deep and superficial nephrons of rats. Lab Invest. 2000 Nov;80(11):1691–700.

7. Weibel ER, Gomez DM. A principle for counting tissue structures on random sections. Journal of Applied Physiology. American Physiological Society; 1962 Mar 1;17(2):343–8.

8. Puelles VG, Douglas-Denton RN, Cullen-McEwen L, McNamara BJ, Salih F, Li J, et al. Design-based stereological methods for estimating numbers of glomerular podocytes. Annals of Anatomy - Anatomischer Anzeiger. 2014 Jan;196(1):48–56.

9. Bertram JF. Counting in the kidney. Kidney international. 2001 Feb;59(2):792–6.

10. Mayhew TM, Gundersen HJ. “If you assume, you can make an ass out of u and me”: a decade of the disector for stereological counting of particles in 3D space. J Anat. 1996;.

11. Beeman SC, Zhang M, Gubhaju L, Wu T, Bertram JF, Frakes DH, et al. Measuring glomerular number and size in perfused kidneys using MRI. AJP: Renal Physiology. 2011 Jun;300(6):F1454–7.

12. Heilmann M, Neudecker S, Wolf I, Gubhaju L, Sticht C, Schock-Kusch D, et al. Quantification of glomerular number and size distribution in normal rat kidneys using magnetic resonance imaging. Nephrol Dial Transplant. 2012 Jan;27(1):100–7.

13. Bennett KM, Zhou H, Sumner JP, Dodd SJ, Bouraoud N, Doi K, et al. MRI of the basement membrane using charged nanoparticles as contrast agents. Magn Reson Med. Wiley Subscription Services, Inc., A Wiley Company; 2008 Sep 1;60(3):564–74.

14. Beeman SC, Cullen-McEwen LA, Puelles VG, Zhang M, Wu T, Baldelomar EJ, et al. MRI-based glomerular morphology and pathology in whole human kidneys. American Journal of Physiology - Renal Physiology. 2014 Jun 1;306(11):F1381–F1390.

15. Baldelomar EJ, Charlton JR, Beeman SC, Hann BD, Cullen-McEwen L, Pearl VM, et al. Phenotyping by magnetic resonance imaging nondestructively measures glomerular number and volume distribution in mice with and without nephron reduction. Kidney Int. 2016 Feb;89(2):498–505.

16. Zalups RK. The Os/+ mouse: a genetic animal model of reduced renal mass. American Journal of Physiology-Renal …. 1993 Jan;264(1 Pt 2):F53–60.

17. Wicksell SD. The Corpuscle Problem. A Mathematical Study of a Biometric Problem. Biometrika. 1925;17(1-2):84–99.

18. Haas CS, Amann K, Schittny J, Blaser B. Glomerular and renal vascular structural changes in α8 integrin-deficient mice. J Am Soc Nephrol. 2003;14(9):2288–96.

19. Cullen-McEwen LA, Armitage JA, Nyengaard JR, Moritz KM, Bertram JF. A design-based method for estimating glomerular number in the developing kidney. Am J Physiol Renal Physiol. 2011 Jun 6;300(6):F1448–F1453.

20. Arsenault MG, Miao Y, Jones K, Sims D, Spears J, Wright GM, et al. Estimation of total glomerular number using an integrated disector method in embryonic and postnatal kidneys. Can J Kidney Health Dis. BioMed Central; 2014 Dec 1;1(1):1–7.

21. Weibel ER. Stereological Methods: Vol. 1. Practical Methods for Biological Morphometry. London: Academic Press; 1979. 1 p.

22. Klein PP. On the Ellipsoid and Plane Intersection Equation. Applied Mathematics. 2012;.

23. Morgan DJ, Jerram DA. On estimating crystal shape for crystal size distribution analysis. Journal of Volcanology and Geothermal Research. 2006;154(1-2):1.

24. Ekblom P. Formation of basement membranes in the embryonic kidney: an immunohistological study. J Cell Biol. Rockefeller Univ Press; 1981 Oct 1;91(1):1–10.

25. Danon D, Goldstein L, Marikovsky Y, Skutelsky E. Use of cationized ferritin as a label of negative charges on cell surfaces. J Ultrastructure Res. 1972;38:500–10.

26. Bertram JF, Young RJ, Seymour AE, Kincaid-Smith P, Hoy W. Glomerulomegaly in Australian Aborigines. Nephrology. Blackwell Publishing Ltd; 1998 Sep 1;4(s2):S46–S53.

27. Barnes N. Publish your computer code: it is good enough. Nature. 2010;467(7317):753.

Appendix- Code Snippets

Publishing source code is important scientific best practice. Open-source software improves scientists' ability to code, enhances peer-review, allows replication, and builds public trust(27). Thus the MATLAB scripts for critical portions of the algorithms are included here.

Smoothing z-stacks to remove mounting artifacts

```
function [smoothed]=smoothStack(varargin)
    %input should be a 3D matrix consisting of a z-stack (single channel)
    %if no input, prompt for a tiff z-stack (single channel)
    %Code by Bradley Hann

    %Parameters
    blurSize=200; %increase to make regions larger
    doPlots = 1; %1 to plat figures, 0 to plot nothing

    %initialize
    if nargin == 0
        image = tifRead();
    elseif nargin ==1 ;
        image = varargin{1};
    end

    height = size(image,1);
    width = size(image,2);
    smoothed = zeros(height,width);
    noSlices = size(image,3);

    %main algorithm
    [~,i]=max(image,[],3);
    gFilt = fspecial('gaussian',blurSize,blurSize/4);
    iBlur= imfilter(i,gFilt,'replicate');
    iBlur = round(iBlur);
    iBlur(iBlur==0)=1;

    for i = 1:height
        for j = 1:width
            smoothed(i,j) = image(i,j,iBlur(i,j));
        end
    end

    if doPlots
        [gx,gy]=imgradientxy(iBlur);
        grad=imgradient(gx,gy);
        grad(grad>.1)=1;
        figure, imshowpair(smoothed(:,:,1),grad,'falsecolor','colorchannels',[1 2 0]);
    end

    function [image]=tifRead()
[file , path]=uigetfile({'*.tif';'*.tiff'},'Select a single-channel tiff image.');
        tifFile = [path file];
        thisInfo = imfinfo(tifFile);
        noImages = numel(thisInfo);
        image = zeros(thisInfo(1).Height,thisInfo(1).Width,noImages);
```

```
        for ii = 1:noImages
            image(:,:,ii)=imread(tifFile,ii,'Info',thisInfo);
        end
    end
end
```

Simulating ellipsoidal profiles

```
function [out]=sliceEllipsoid(varargin)
    %optional input is (Volume, [axialRatio1 axialRatio2])
    %code is based on the method of Klein, Applied Mathematics, 2012, 3, 1634-1640

    if nargin == 0
        vol = 2.5*10^5;
        ratios = [1 1];
    elseif nargin == 2
        vol = varargin{1};
        ratios = varargin{2};
    end

    %main

        el = generateEllipsoid(vol,ratios);
        [n,q] = generatePlane(el);
        d = calcD(n,q,el);
        beta1=roots([1,-1*sumBeta(n,el),prodBeta(n,el)]);
        beta1 = real(beta1);
        beta1 = beta1(find(beta1>0,1,'first'));
        beta2=prodBeta(n,el)/beta1(1);
        A = sqrt((1-d)/beta1);
        B = sqrt((1-d)/beta2);
        area = pi()*A*B;

    %save stuff
    out = struct( ...
        'el',el ...
        ,'n', n ...
        ,'q', q ...
        ,'d', d ...
        ,'vol', vol ...
        ,'elRatios' , [1, ratios] ...
        ,'beta', [beta1,beta2] ...
        ,'A', A ...
        ,'B', B ...
        ,'area', area ...
        ,'axRatio' , max([A/B , B/A])...
        ,'l' , sqrt(area/pi()) ...
        );

function [out] = generateEllipsoid(vol,ratios)
        %generate random ellipse at the origin
        a = (3*vol/(4*pi()*prod(ratios)))^(1/3);
        b = ratios(1)*a;
        c = ratios(2)*a;
        out = [a b c];
end

    function [const] = sumBeta(n,el)
```

```
        a = el(1)^-2;
        b = el(2)^-2;
        c = el(3)^-2;
        const = (n(1)^2)*(b + c) + (n(2)^2)*(c+a) + (n(3)^2)*(a+b);
    end

    function [const] = prodBeta(n,el)
        t(1) = (n(1)^2)/(prod(el([2,3]))^2);
        t(2) = (n(2)^2)/(prod(el([1,3]))^2);
        t(3) = (n(3)^2)/(prod(el([1,2]))^2);
        const = sum(t);
    end

    function [const] = calcD(n,q,el)
        kappa = sum(q.*n)/sqrt(sum(n.^2));
        num = sum(n.^2);
        den = sum((el.^2).*(n.^2));
        const = (kappa^2)*num/den;
    end

    function [pnv, point] = generatePlane(ellipse)

        %generate random plane that bisects the ellipse
        pn = rand(1,2)*2*pi();
        pnv = [sin(pn(1))*cos(pn(2)) , sin(pn(1))*sin(pn(2)) , cos(pn(1))];
        badPoint = 1;
        count = 0;
        while(badPoint)
            point = (2*rand(1,3)-1).*ellipse;
            isIn = sum((point.^2)./(ellipse.^2));
            count=count + 1;
            if (isIn < 1 ) || (count>100)
                badPoint = 0;
            end
        end
        %d = -1*sum(pn.*point);
        %out = [pnv d];
    end
end
```

Unfolding Algorithm

```
function [out]=histCorrectPublish(ls,varargin)

% First input must be a column of measured glomerular radii
% Optional input-value pairs:
% 'noisy': 1 will do plots, 0 will not. Default 0
% 'smallest': assumed smallest possible particle radius. Default 20um
% 'nBins': number of bins to use. Default 18.
% 'maxBin': largest possible glomerular radius. Default 60
%
% Output is struct with the following fields:
% 'hists':2D matrix of the histogram at each iteration
% 'finalProfile': profile histogram after the algorithm (negative values of small glomeruli are the 'lost caps')
% 'original': original normalized histogram of profile radii
% 'corrected': normalized histogram of profile radii including the calculated 'lost caps'
% 'centers': output histogram centers in terms of radius
% 'rHist': hitogram of particle radii without correction for size
% 'sizeRhist': histogram of particle radii after correcting for the increased probability of sampling larger glomeruli
```

```
%
% Code by Bradley Hann


p = inputParser;
addOptional(p,'noisy',0,@isnumeric);
addOptional(p,'smallest',20,@isnumeric);
addOptional(p,'nBins',18,@isnumeric);
addOptional(p,'maxBin',60,@isnumeric);
addRequired(p,'ls',@isnumeric);
parse(p,ls,varargin{:});

norm = @(x) x./sum(x);
smallest=p.Results.smallest;
noisy = p.Results.noisy;
gloms = p.Results.ls;
maxBin=p.Results.maxBin;
gloms=gloms(gloms>10);
nBins = p.Results.nBins;

%Initialize things that will be output,
%itHists (particles), itProfs (profiles), and itPsi (PDF) are only used
%to save data for possible future inspection.
itHists=zeros(nBins);
itProfs=zeros(nBins);
itPsi=zeros(nBins);
rHist=zeros(1,nBins);

%Bin index is the upper bound of the bins
binIdx = linspace(0,maxBin,nBins+1);
binIdx = binIdx(2:end);
dbin=binIdx(3)-binIdx(2);
binCent = binIdx-dbin/2;

%The MATLAB function hist uses bin centers as an input
[start,~]=hist(gloms,binCent);
original=start;

%The variable 'smallest' is the smallest possible profile,
%this guards against segmentation artifacts
small=find(binCent<smallest,1,'last');
start(1:small)=0;
start=start/sum(start);

%Normalize the original histogram, with small profiles removed,
%and save to an extra variable for possible future use
origFlattened=start;

for i = 1:sum(start>0)
    itHists(i,:)=start;
    currentBin = nBins-(i-1);
    if (start(currentBin)>0) || (currentBin>10) %occasionally a lone large profile will cause the loop to stop prematurely
        R=binIdx(currentBin);
        r=(1:currentBin)*dbin;
        for j = 1:currentBin
            psi(j)=psiInt(r(j),R,dbin);
        end
        itPsi(i,1:numel(psi))=psi;
```

```
        psi = psi*(start(currentBin)/psi(end));
        rHist(currentBin)=sum(psi);
        profiles=[psi zeros(1,nBins-numel(r))]; %zero fill array
        itProfs(i,:)=profiles;
        start=start-profiles;
        clear psi
    end
end
rHist(rHist<0)=0;
corrected = origFlattened;
corrected(1:small+1)=corrected(1:small+1)-start(1:small+1);

out = struct( ...
    'hists',itHists ...
    , 'finalProfile', start ...
    , 'original' , norm(original) ...
    , 'centers', binCent...
    , 'rHist', real(rHist) ...
    , 'corrected', corrected ...
    , 'sizeRhist' , real(sizeCorrect(rHist,binCent)) ...
    , 'originalData' , ls ...
    );

if noisy
    figure; hold on;
    plot(out.centers,out.original/sum(out.original),'x-')
    plot(out.centers,out.corrected,'xr-')
    xlabel('Profile radius (\mum)')
    ylabel('frequency')
    legend('Original','Corrected','location','northwest');
    hold off

    figure; plot(out.centers,out.rHist,'x-')
    xlabel('Glomerular radius (\mum)')
    ylabel('frequency')
    title('Original Distribution')
end

    function [outHist]= sizeCorrect(inHist,centers)
        histMean=sum(norm(inHist).*centers);
        factors = centers/histMean;
        outHist = inHist./factors;
    end

    function [out]=psiInt(r,R,dbin)
        a = -sqrt(R^2-r^2)/R;
        b = -sqrt(R^2-(r-dbin)^2)/R;
        out = a-b;
    end
end
```